Characterizing exoplanet atmospheres with SCALES medium-spectral-resolution angular differential imaging

Aditi Desai^a, Steph Sallum^a, Ravinder Banyal^b, Natalie Batalha^c, Natasha Batalha^d, Geoff Blake^e, Tim Brandt^f, Zack Briesemeister^d, Katherine de Kleer^e, Imke de Pater^g, Josh Eisner^h, Wen-fai Fongⁱ, Tom Greene^d, Mitsuhiko Honda^j, Isabel Kain^c, Charlie Kilpatrickⁱ, Mackenzie Lach^a, Mike Liu^k, Bruce Macintosh^c, Raquel A. Martinez^a, Dimitri Mawet^e, Brittany Miles^h, Caroline Morley^l, Diana Powell^m, Patrick Sheehanⁿ, Andrew J. Skemer^c, R. Deno Stelter^c, Jordan Stone^p, Arun Surya^b, Sivarani Thirupathi^b, Kevin Wagner^h, and Yifan Zhou^q

^aUC Irvine, Irvine, CA, USA ^bIndian Institute of Astrophysics, Koramangala, Bengaluru, India ^cUC Santa Cruz, Santa Cruz, CA, USA ^dNational Aeronautics and Space Administration, USA ^eCalifornia Institute of Technology, Pasadena, CA, USA ^fUC Santa Barbara, Santa Barbara, CA, USA gUC Berkeley, Berkeley, CA, USA ^hUniversity of Arizona, Tucson, AZ, USA ⁱNorthwestern University, Evanston, IL, USA ^jOkayama University of Science, Okayama, Japan ^kUniversity of Hawaii, Honolulu, HI, USA ¹UT Austin, Austin, TX, USA ^mUniversity of Chicago, Chicago, IL, USA ⁿNational Radio Astronomy Observatory, Socorro, NM, USA ^pUS Naval Research Laboratory, Washington, D.C., USA ^qUniversity of Virginia, Charlottesville, USA

ABSTRACT

SCALES (Slicer Combined with Array of Lenslets for Exoplanet Spectroscopy) is a high-contrast lenslet-based integral field spectrograph (IFS) designed to characterize exoplanet atmospheres in the 2 - 5 micron wavelength range. The SCALES medium-resolution mode provides the ability to characterize exoplanets at increased spectral resolution via the use of a lenslet subarray with a 0.34 x 0.36 arcsecond field of view and an image slicer. We use the SCALES simulator scalessim to generate high-fidelity mock observations of planets in the medium-resolution mode that include realistic Keck adaptive optics performance, as well as other atmospheric and instrumental noise effects, to simulate planet detections, and then employ angular differential imaging to extract the planet spectra. Analyzing the recovered spectra from these simulations allows us to quantify the effects of systematic noise sources on planet characterization, in particular residual speckle noise following angular differential data processing. We use these simulated recovered spectra to explore SCALES' ability to constrain molecular abundances and disequilibrium chemistry in giant exoplanet atmospheres.

Keywords: SCALES, high-contrast spectroscopy, exoplanet characterization, angular differential imaging

1. INTRODUCTION

SCALES (Slicer Combined with Array of Lenslets for Exoplanet Spectroscopy) is a 2 - 5 micron high-contrast lenslet-based integral field spectrograph (IFS) that is being constructed for the purpose of characterizing exoplanet atmospheres. A novel aspect of SCALES is its medium-resolution mode, which uses a lenslet subarray with a 0.34 x 0.36 arcsecond field of view in series with an image slicer to allow for exoplanet characterization at increased spectral resolution. At medium resolution, SCALES has K, L, and M band modes with resolution R > 3500, and is specifically designed to constrain effective temperature to within 10 K, metallicity ([M/H]) ratios to within \sim 0.1, and log abundances of H₂O, CH₄, NH₃ to within \sim 0.1 for planets as cold as 300 K. Additionally, for planets hotter than 500 K, the SCALES medium-resolution mode is designed to measure log abundances of molecules like CO, CO₂, and PH₃ to within \sim 1.

Unlike most traditional observing modes, the field of view in the SCALES medium-resolution mode is not centered on the planet host star. The instrument instead guides on the exoplanet by following the star-planet system's parallactic rotation, providing a series of images of the planet and noise from the star that differs in each image as the respective positions of the star and planet change.

Here we look to determine the extent of SCALES' ability to constrain molecular abundances and chemical disequilibrium using the medium-resolution mode. In order to explore SCALES' sensitivity, high-fidelity mock observations of planets are simulated using the SCALES simulator scalessim that include speckle noise from their host stars, as well as other atmospheric and instrumental noise effects, while varying a variety of model parameters.³ For the purposes of this project, all simulations were carried out for the SCALES medium-resolution M band mode. The M band spans wavelengths from 4.5 microns to 5.2 microns and has a resolving power of R = 7000.

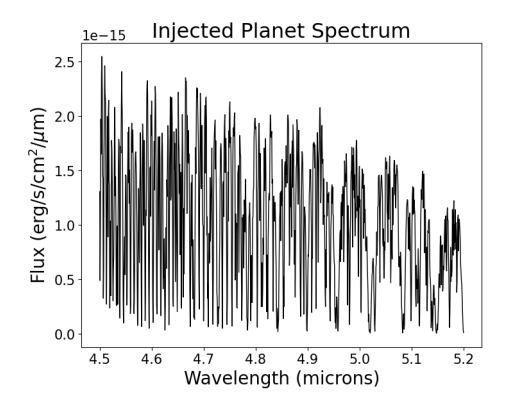
2. METHODS

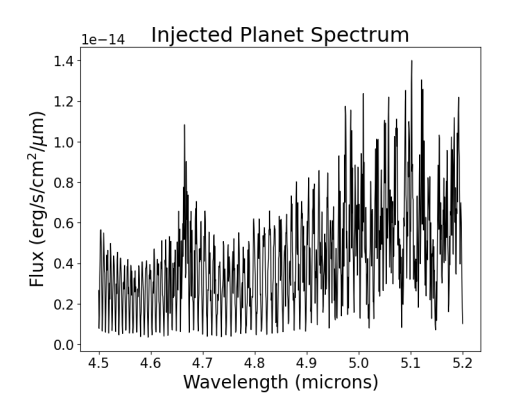
To simulate mock SCALES medium-resolution observations, we use scalessim to inject the spectrum of a planet (see Fig. 1 for examples) in a different location over a range of parallactic angles (η) and the spectrum of its host star, with the planet always placed in the center of the frame and the star being placed at a fixed distance away. The injected planet spectra are from the Sonora Elf Owl model grid, which consists of radiative-convective equilibrium model atmospheres with vertical mixing induced disequilibrium chemistry. The variable parameters in the grid are effective temperature ($T_{\rm eff}$), gravity ($\log(g)$), vertical eddy diffusion coefficient ($\log(Kzz)$), atmospheric metallicity ([M/H]), and carbon-to-oxygen ratio (C/O).

For a given set of log(Kzz), $T_{\rm eff}$, log(g), [M/H], and C/O values, the injected planet is placed at a 500 mas separation from its 3000 K host star, which is modeled using a PHOENIX spectrum.⁵ scalessim generates a spectrally oversampled datacube of 17 by 18 spaxels at 34001 wavelengths between 1.9 and 5.3 microns, and 13 of these cubes are generated with independent noise realizations and changing Keck PSFs, representing 13 images at different parallactic angles over a range of $\eta = -60^{\circ}$ to $\eta = 60^{\circ}$. The total integration time for each set of parameters is 2 hours for hot planets ($T_{\rm eff} > 600$ K) and 20 hours for cold planets ($T_{\rm eff} < 600$ K). The relationship $R = 7000 = \lambda/\Delta\lambda$ where $\lambda = \frac{5.2 + 4.5}{2} = 4.85$ microns is then used to rebin the oversampled datacube to the resolving power of the M band medium-spectral-resolution mode.

Once the mock observations have been generated, angular differential imaging (ADI) is used to process the images and extract the planet signal. ADI is a high-contrast imaging technique that reduces quasi-static speckle noise, and consequently aides in the detection of companions.⁶ In traditional ADI, the field of view rotates with respect to the instrument, as observations of the host star are made and a sequence of images is taken with the instrument derotater turned off. The average speckle noise in each image is captured in a reference point-spread-function (PSF), which is constructed from images from the same sequence. Once constructed, the reference PSF is subtracted from each science image, and the residual images are combined after being rotated to align the field.

For SCALES medium-resolution images, traditional ADI cannot be applied, since the field of view is not centered on the host star and as a result, there is no rotation involved. In order to employ ADI here, a reference PSF that captures the average speckle noise in each image is generated by defining an exclusion zone at the center of each science image that ignores light from the planet at each wavelength and η value. Each image





(a) Injected spectrum of a planet with $T_{\rm eff}=400$ K, $\log({\rm Kzz})=7.0,\ \log({\rm g})=31.0,\ [{\rm M/H}]=-1.0,\ {\rm C/O}=2.5.$

(b) Injected spectrum of a planet with $T_{\rm eff}=1000$ K, $\log({\rm Kzz})=9.0,\ \log({\rm g})=31.0,\ [{\rm M/H}]=0.0,\ {\rm C/O}=0.5$

Figure 1: Sample injected Sonora Elf Owl planet spectra used in scalessim when generating mock-observations. The left panel shows a cold planet and the right panel shows a hot planet.

is then placed at its corresponding η value with respect to the host star and the mean of all the overlapping images in a given region is calculated. Fig. 2 shows a schematic of the reference PSF construction method and an example reference PSF.

The planet spectrum is extracted by injecting negative Gaussians to attempt to remove the planet signal and then minimizing the ADI-processed residuals to determine the flux at each wavelength.⁸ The planet flux for a given wavelength is assumed to be equal at all values of η . The total number of counts collected from the planet is then the sum of the best-fit Gaussian times the number of parallactic angles.

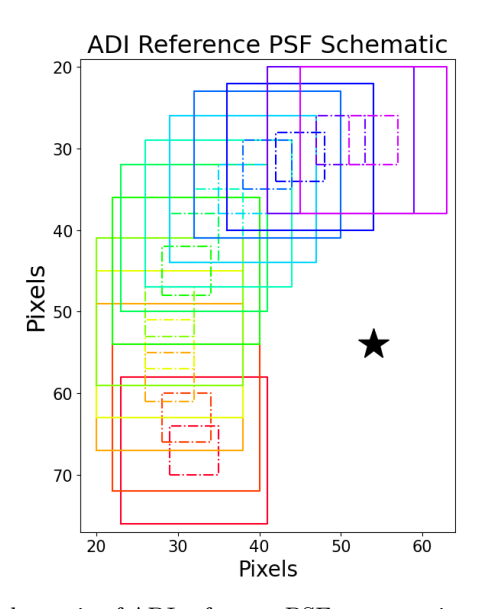
We also simulate telluric calibrators in order to correct for sky transmission and flux calibrate the planet spectra. The spectrum of an A star is sent through scalessim in the same way as the planet spectra, with the star placed at the center of the frame. The generated datacube, rebinned to the M band resolving power, is then compared to a template spectrum to calculate the telluric correction. We use the resulting ratio to convert the recovered planet spectra to flux units.

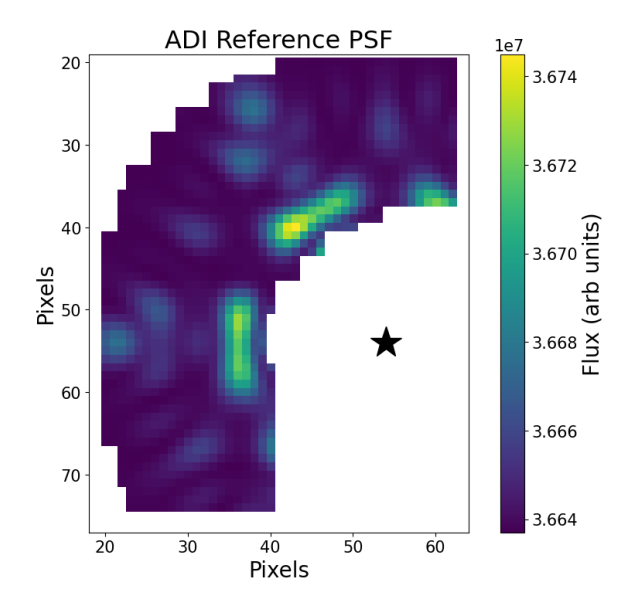
The error for each wavelength is determined by calculating the standard deviation of the images at each η value individually, multiplying each of them by the square root of the number of pixels occupied by the planet PSF, adding them in quadrature, and converting the resulting value to flux units. For the purposes of this project, at wavelengths where the signal-to-noise ratio (SNR) has a value less than 1, we exclude the flux value from subsequent fitting. The SNR here is determined by comparing the best-fit Gaussian to the calculated error.

Once a spectrum has been recovered along with the respective noise for each flux value, a chi-squared analysis is performed to to find the best-fit model parameters for the simulated observed spectrum, and to determine whether the correct parameters can be recovered. Each extracted spectrum is compared with models in the Sonora Elf Owl model grid. For each extracted spectrum, χ^2 values are calculated to compare the spectrum to the grid of models. The best-fit χ^2 value is rescaled to be equal to 1005, or the number of degrees of freedom,

Sigma	1σ	2σ	2σ 3σ		5σ	
k = 5	5.89	11.31	18.21	26.77	37.09	

Table 1: Chi-squared distribution table up to 5σ where k is the number of degrees of freedom in the χ^2 distribution. The χ^2 values calculated for each extracted spectrum with models in the Elf Owl grid are compared to these values to determine how well each parameter can be constrained. For example, any parameters with χ^2 values between 1005.0 and 1010.89 are allowed at 1σ .





(a) Schematic of ADI reference PSF construction. The solid squares represent the images, the dash-dotted squares represent the exclusion zone for each image in the sequence, and the black star represents the host star PSF. The color progression indicates that each image is taken at a different value of η .

(b) An example ADI reference PSF for a planet with $\log(\mathrm{Kzz}) = 7.0$, $T_{\mathrm{eff}} = 400~\mathrm{K}$, $\log(\mathrm{g}) = 31.0$, $[\mathrm{M/H}] =$ -1.0, $\mathrm{C/O} = 2.5$ around a 3000 K star. All light within the exclusion zone has been eliminated from each individual image over all η values and all wavelengths, and the remaining noise was averaged over the η values.

Figure 2: An ADI reference PSF constructed with 13 η values and a 500-mas planet-star separation.

which is the difference between the number of data points, 1010, and parameters in this fit, 5. The χ^2 values are then analyzed using the values in Table 1 in order to establish parameter constraints.

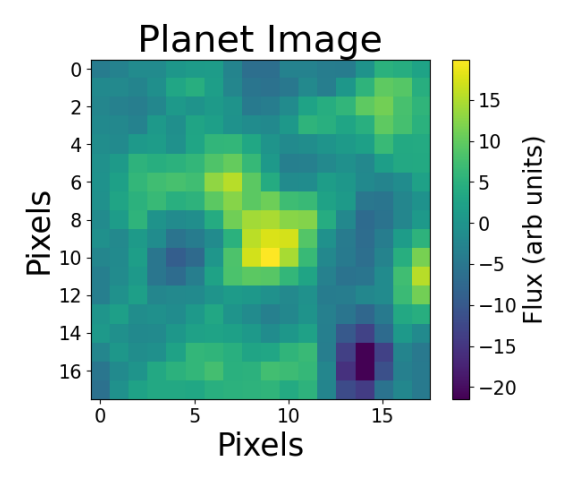
3. RESULTS AND DISCUSSION

Figure 3 shows two resulting images and spectra obtained after employing ADI on the mock observations generated by scalessim. Both the deconvolved planet images in Fig. 3a and Fig. 3c are pictured at $\lambda = 4.665~\mu m$ to demonstrate that detections are visible at individual wavelengths.

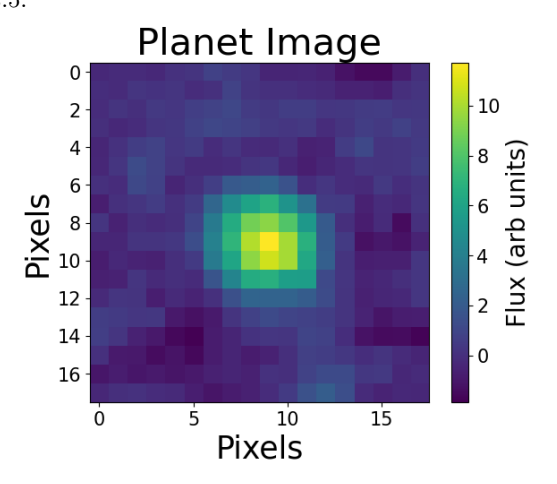
In general, the overall features and shape of the injected spectra are recovered through the ADI processing, as can be seen in Fig. 3b and Fig. 3d. However, there is significant discrepancy in the magnitude of the recovered fluxes for colder planets. In Fig. 4, the recovered and injected flux values are compared directly, where a slope of 1 indicates a perfect recovery. Fig. 4a indicates that there is a systematic shift where recovered flux values are lower than the injected values for the cold planet, while Fig. 4b suggests that this effect is significantly smaller for the hot planet, though not negligible. We can also see that some planet fluxes are systematically overestimated for the hot planet.

One explanation for the underestimated fluxes is that some amount of oversubtraction is occurring during the ADI processing and is more significant for cold planets where the SNR is lower. The issue of self-subtraction is a known effect in traditional ADI as well — if there is planet light that is not excluded while generating the reference PSF, that flux can be subtracted off during ADI processing, resulting in an overall decrease in flux in the residual images. The changing speckle noise from the use of changing Keck PSFs could also be a source of error, resulting in relative dips and spikes in the best-fit flux values. A potential approach to mitigate these effects is to perform throughput measurements, which will be the subject of future papers.

Figure 5 presents a selection of chi-squared surfaces that show how the χ^2 values vary as different pairs of atmospheric parameters are varied during fits to the recovered spectra. Table 2 presents these same results with the χ^2 -measured error bars for the best-fits made explicit. The color scale indicates the significance level with

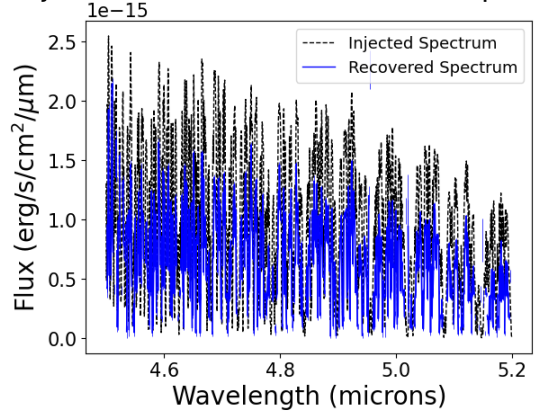


(a) Deconvolved planet image summed over all η values at $\lambda=4.665~\mu m$ for a planet with $T_{\rm eff}=400$ K, $\log(Kzz)=7.0,~\log(g)=31.0,~[M/H]=-1.0,~C/O=2.5.$



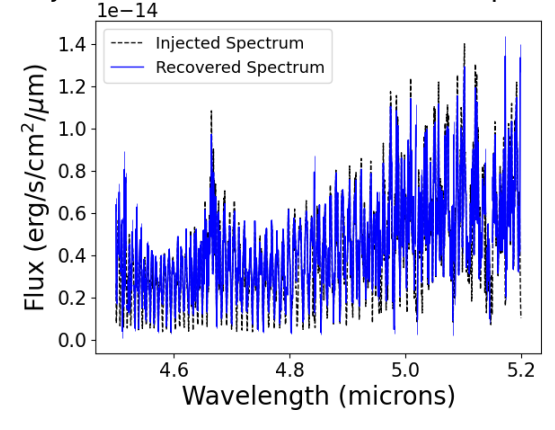
(c) Deconvolved planet image summed over all η values at $\lambda=4.665~\mu m$ for a planet with $T_{\rm eff}=1000$ K, $\log(Kzz)=9.0,~\log(g)=31.0,~[M/H]=0.0,~C/O=0.5.$

Injected and Recovered Planet Spectrum



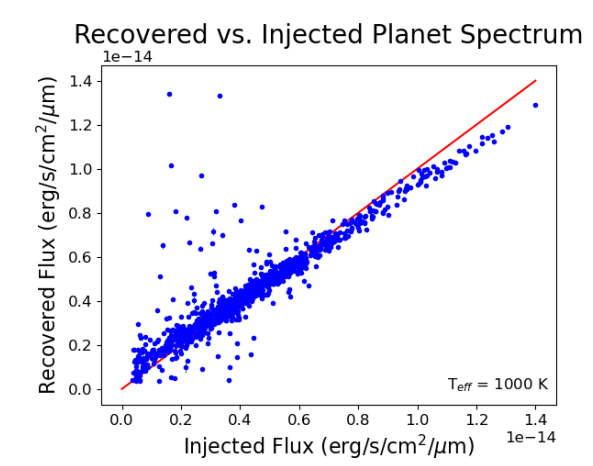
(b) Injected model spectrum with the recovered planet spectrum overlaid with error bars for a planet with $T_{\rm eff}=400~\rm K,$ $\log(\rm Kzz)=7.0,$ $\log(\rm g)=31.0,$ $[\rm M/H]=-1.0,$ $\rm C/O=2.5.$

Injected and Recovered Planet Spectrum



(d) Injected model spectrum with the recovered planet spectrum overlaid with error bars for a planet with $T_{\rm eff}=1000$ K, $\log(Kzz)=9.0$, $\log(g)=31.0$, [M/H]=0.0, C/O=0.5.

Figure 3: Examples of recovered planet images and spectra for various parameter combinations.



- (a) Recovered model spectrum versus injected planet spectrum plotted with error bars for a planet with $T_{\rm eff}=400~K,\,\log(Kzz)=7.0,\,\log(g)=31.0,\,[M/H]=-1.0,\,C/O=2.5.$
- (b) Recovered model spectrum versus injected planet spectrum plotted with error bars for a planet with $T_{\rm eff}$ = 1000 K, $\log({\rm Kzz})$ = 9.0, $\log({\rm g})$ = 31.0, $[{\rm M/H}]$ = 0.0, ${\rm C/O}$ = 0.5.

Figure 4: Direct comparison between the injected and recovered flux values for two models. The red line in each plot has a slope of 1 and represents a perfect recovery.

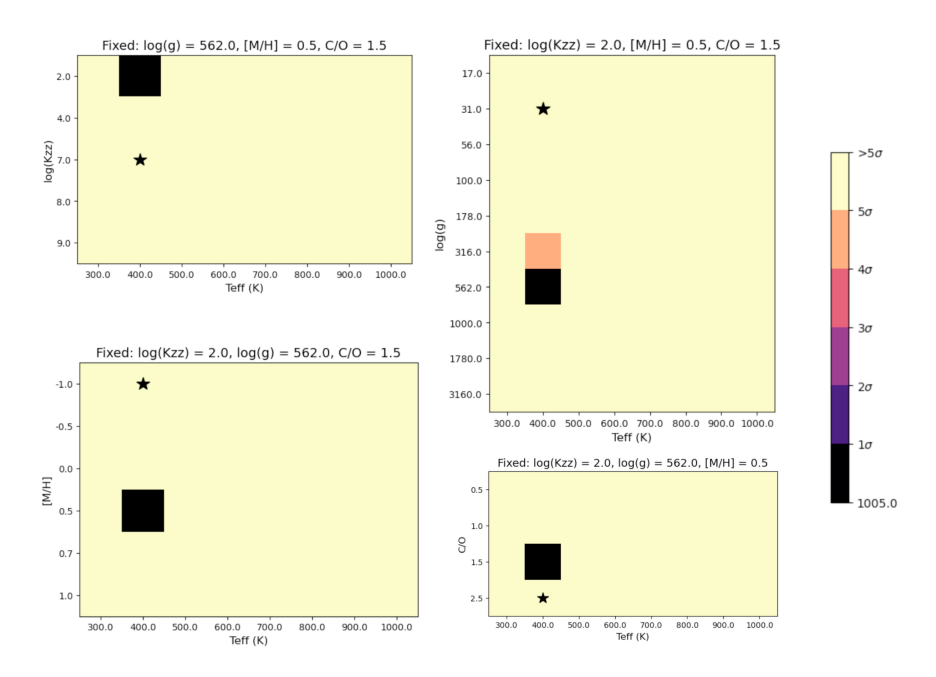
which each set of parameters is allowed by the fit. The best-fit models for the extracted spectra are not the true injected models for either the hot or cold planet. For $\log(\text{Kzz})$ and $\log(g)$ in particular, the best-fit values tend to differ greatly from the true values regardless of planet temperature, while there is slightly less variation for [M/H] and C/O, with the true value of [M/H] being allowed within 5σ and that of C/O being allowed within 1σ for the hot planet. The only parameter for which the true value is consistently allowed within 1σ for both the hot and cold planet is T_{eff} . These discrepancies are likely the result of the systematic errors illustrated in Fig. 4, and we will explore strategies to mitigate them in future papers.

4. CONCLUSIONS

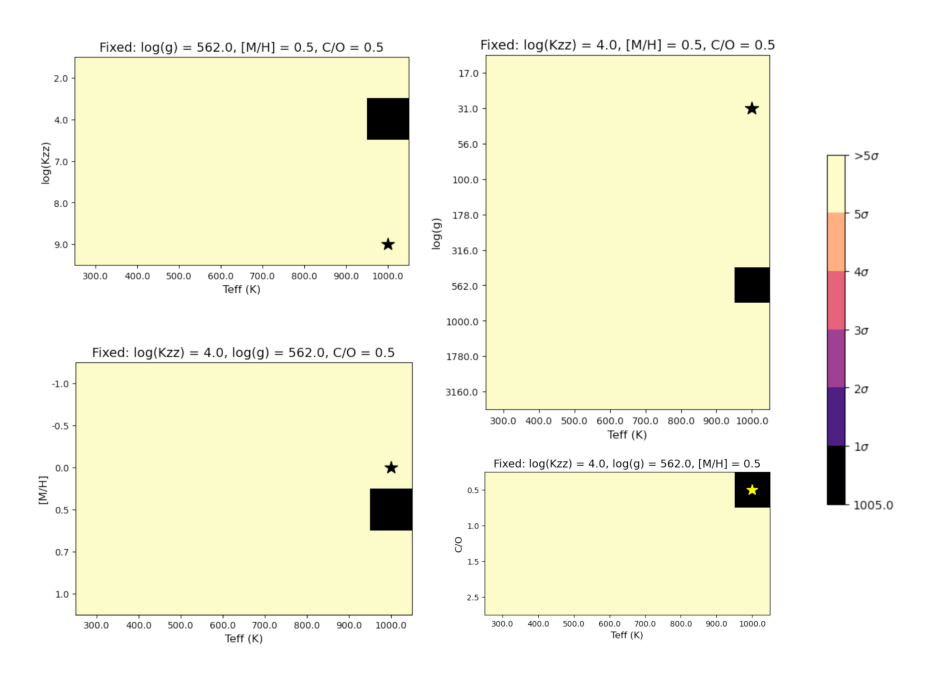
In this paper, we presented simulated planetary atmosphere characterizations with the SCALES M band medium-resolution mode. These simulations explore the effects of quasi-static speckle removal using a modified approach to angular differential imaging tailored for the unique SCALES field of view. The preliminary results indicate that planet temperature is generally well-constrained regardless of how hot or cold the planet is, while metallicity and the carbon-to-oxygen ratio can be constrained relatively well for hot planets, and the ability to place constraints on planet gravity and the vertical eddy diffusion coefficient tends to vary more with planet temperature. Hotter planets are also generally more reliably constrained overall than colder planets. These discrepancies are likely caused by the systematic errors present in the recovered spectra, which may be caused by oversubtraction, imperfect subtraction of changing speckle noise, or a combination of both.

		Injected Model Parameters					Best-Fit Model Parameters				
		log(Kzz)	T _{eff} (K)	log(g)	[M/H]	C/O	$\log(\text{Kzz})$	T _{eff} (K)	log(g)	[M/H]	C/O
	1	7.0	400.0	31.0	-1.0	2.5	$2.0 \pm < 2.0$	$400.0 \pm < 100.0$	$562.0\pm^{<246.0}_{246.0}$	$0.5 \pm < 0.2$	$1.5 \pm < 0.5$
ſ	2	9.0	1000.0	31.0	0.0	0.5	$4.0\pm^{3.0}_{<2.0}$	$1000.0 \pm < 100.0$	$562.0\pm^{<246.0}_{384.0}$	$0.5\pm^{<0.5}_{0.5}$	$0.5 \pm < 0.5$

Table 2: Table of fit results. The "Injected Model Parameters" column indicates the true parameter values of the injected model, and the "Best-Fit Model Parameters" column indicates the best fit values for the extracted spectrum based on the chi-squared analysis. The errors here indicate the parameter values allowed at 5σ . The errors accompanied by < symbols have values less than the spacing between subsequent points in the Elf-Owl grid. Note that in Row 1, the best-fit $\log(\text{Kzz})$ value is at the lower limit of the grid.



(a) Chi-squared surfaces for a planet with $T_{\rm eff}=400~{\rm K},\,\log({\rm Kzz})=7.0,\,\log({\rm g})=31.0,\,[{\rm M/H}]=-1.0,\,{\rm C/O}=2.5.$ Here, the parameters not being varied have been held at their best-fit values: $T_{\rm eff}=400~{\rm K},\,\log({\rm Kzz})=2.0,\,\log({\rm g})=562.0,\,[{\rm M/H}]=0.7,\,{\rm C/O}=0.5.$ The black star in each plot is placed at the position of the true values of the varied parameters.



(b) Chi-squared surfaces for a planet with $T_{\rm eff}=1000~K$, $\log(Kzz)=9.0$, $\log(g)=31.0$, [M/H]=0.0, C/O=0.5. Here, the parameters not being varied have been held at their best-fit values: $T_{\rm eff}=1000~K$, $\log(Kzz)=4.0$, $\log(g)=562.0$, [M/H]=0.5, C/O=0.5. The black/yellow star in each plot is placed at the position of the true values of the varied parameters.

Figure 5: Chi-squared surfaces demonstrating the best-fit parameters for two sample planets.

More work must be done in the future to perform more robust chi-squared analyses on a larger number of extracted spectra where more parameters are varied. We must also account for effects of possible oversubtraction and changing speckle noise resulting in imperfect recovered flux values. Future work will build on this ADI approach to measure and correct for throughput, which will likely mitigate these systematic errors. More realistic simulations must also be generated, as not all potential noise sources have been explored thoroughly, and changing sky transmission/emission with airmass and conditions have not been explicitly considered. Future work will involve enhancements such as variable sky transmission/emission, adding spectral differential imaging, exploring the K and L bands, and performing joint fits to K, L, and M band spectroscopy of single planets. These simulations will ensure that early SCALES observations are executed as efficiently as possible, and are scientifically productive.

ACKNOWLEDGMENTS

We are grateful to the Heising-Simons Foundation, the Alfred P. Sloan Foundation, and the Mt. Cuba Astronomical Foundation for their generous support of our efforts. This project also benefited from work conducted under the NSF Graduate Research Fellowship Program. S.S. is supported by the National Science Foundation under MRI Grant No. 2216481. R.A.M is supported by the National Science Foundation MPS-Ascend Postdoctoral Research Fellowship under Grant No. 2213312.

REFERENCES

- [1] Stelter, R. D., Skemer, A. J., Kupke, R., Bourgenot, C., Martinez, R. A., and Sallum, S. S., "Weighing exo-atmospheres: a novel mid-resolution spectral mode for SCALES," in [Ground-based and Airborne Instrumentation for Astronomy IX], Evans, C. J., Bryant, J. J., and Motohara, K., eds., 12184, 1218445, International Society for Optics and Photonics, SPIE (2022).
- [2] Sallum, S., Skemer, A., Stelter, D., Banyal, R., Batalha, N., Batalha, N., Blake, G., Brandt, T., Briesemeister, Z., de Kleer, K., de Pater, I., Desai, A., Eisner, J., fai Fong, W., Greene, T., Honda, M., Jensen-Clem, R., Kain, I., Kilpatrick, C., Kupke, R., Lach, M., Liu, M. C., Macintosh, B., Martinez, R. A., Mawet, D., Miles, B., Morley, C., Powell, D., Sethuram, R., Sheehan, P., Spilker, J., Stone, J., Surya, A., Thirupathi, S., Unni, A., Wagner, K., and Zhou, Y., "The slicer combined with array of lenslets for exoplanet spectroscopy (SCALES): driving science cases and expected outcomes," in [Techniques and Instrumentation for Detection of Exoplanets XI], Ruane, G. J., ed., 12680, 1268003, International Society for Optics and Photonics, SPIE (2023).
- [3] Briesemeister, Z., Sallum, S., Skemer, A., Stelter, R. D., Hinz, P., and Brandt, T., "End-to-end simulation of the SCALES integral field spectrograph," in [Ground-based and Airborne Instrumentation for Astronomy VIII], Evans, C. J., Bryant, J. J., and Motohara, K., eds., 11447, 114474Z, International Society for Optics and Photonics, SPIE (2020).
- [4] Mukherjee, S., Fortney, J., Morley, C., Batalha, N., Marley, M., Karalidi, T., Visscher, C., Lupu, R., Freedman, R., and Gharib-Nezhad, E., "The sonora substellar atmosphere models. iv. elf owl: Atmospheric mixing and chemical disequilibrium with varying metallicity and c/o ratios (l- type models)," (2023).
- [5] Husser, T., von Berg, S. W., Dreizler, S., Homeier, D., Reiners, A., Barman, T., and Hauschildt, P. H., "A new extensive library of phoenix stellar atmospheres and synthetic spectra," *A&A* **553**, A6 (2013).
- [6] Marois, C., Lafrenière, D., Doyon, R., Macintosh, B., and Nadeau, D., "Angular differential imaging: A powerful high-contrast imaging technique," The Astrophysical Journal 641, 556–564 (2006).
- [7] Desai, A., Sallum, S. E., Banyal, R., Batalha, N., Batalha, N., Blake, G., Brandt, T., Briesemeister, Z., de Kleer, K., de Pater, I., Eisner, J., fai Fong, W., Greene, T., Honda, M., Kain, I., Kilpatrick, C., Lach, M., Liu, M., Macintosh, B., Martinez, R. A., Mawet, D., Miles, B., Morley, C., Powell, D., Sheehan, P., Skemer, A. J., Spilker, J., Stelter, R. D., Stone, J., Surya, A., Thirupathi, S., Wagner, K., and Zhou, Y., "Simulating medium-spectral-resolution exoplanet characterization with SCALES angular/reference differential imaging," in [Techniques and Instrumentation for Detection of Exoplanets XI], Ruane, G. J., ed., 12680, 1268023, International Society for Optics and Photonics, SPIE (2023).

- [8] Lagrange, A. M., Bonnefoy, M., Chauvin, G., Apai, D., Ehrenreich, D., Boccaletti, A., Gratadour, D., Rouan, D., Mouillet, D., Lacour, S., and Kasper, M., "A Giant Planet Imaged in the Disk of the Young Star β Pictoris," *Science* **329**, 57 (July 2010).
- [9] Milli, J., Mouillet, D., Lagrange, A.-M., Boccaletti, A., Mawet, D., Chauvin, G., and Bonnefoy, M., "Impact of angular differential imaging on circumstellar disk images," AA 545, A111 (2012).
- [10] Esposito, T. M., Fitzgerald, M. P., Graham, J. R., and Kalas, P., "Modeling self-subtraction in angular differential imaging: Application to the hd 32297 debris disk," *The Astrophysical Journal* **780**, 25 (Dec. 2013).